Transactions D:
Computer Science & Engineering and
Electrical Engineering
Vol. 16, No. 2, pp. 145–156

SCIENTIA
IRANICA

Harmonic Content and Relaxation Resonant Frequency of a Modulated Laser Diode

H. Zandi[1], M. Bavafa[1], M.R. Chamanzar[1] and S. Khorasani[1,*]

Abstract. *In this paper, an analysis of the harmonic contents of the optical output power for an in-plane single mode laser diode is performed, and the results are described in detail. In the first step, the absolute value of power for each harmonic is obtained in terms of various laser diode parameters, and the variations of external parameters, such as modulation current, bias current and frequency, are discussed. The analysis is done by direct solution of the rate equations of an arbitrary laser diode for carrier and photon densities. It is known that the optical power has a nonlinear dependence on frequency, and the maximum optical power of each harmonic is attained in its resonance frequency. The resonant frequency is shown to be tunable by the bias current; thus we obtain exact expressions for the output power of various harmonics, allowing better optimization to gain improved results. We extend the approach to higher harmonics, and numerically calculate the Total Harmonic Distortion (THD) versus major parameters, such as frequency, bias current and modulation current. Furthermore, we find optimal operation points in which the desired characteristics of the laser diode can be achieved. It is also possible for the sequence for every arbitrary single-mode laser structure to be developed by the approach presented in this work.*

Keywords: *Laser diode; Optical modulation; Relaxation resonant frequency; Total harmonic distortion.*

INTRODUCTION

The rate equations of a semiconductor laser diode [1] present nonlinear distortions to the output optical power versus input current. This fact can be of importance in the transmission of data in the form of amplitude modulation, and can limit the available bandwidth for large-signal modulation ratios.

For the first time, optical modulation has been used by Lance et al. [2] to determine the intrinsic frequency response of a laser diode. The analysis of nonlinear distortions from a directly current-modulated AlGaAs laser diode under microwave intensity modulation has been done by Way [3]. He simulated second harmonics, two-tone third-order intermodulation, multicarrier intermodulation and intermodulation, due to two arbitrarily separated tones, which were noted to match well with corresponding measured results. Lin et al. [4] performed a measurement and modeling of harmonic distortion in InGaAsP distributed feedback lasers, and noticed that at low modulation frequencies ($\sim$ 50 MHz), the second harmonic distortion exhibits a minimum at a certain bias current, while the minimum was not observed at higher modulation frequencies ($\sim$ 1 GHz). Biswas et al. [5] analyzed the nonlinear optical response of a laser diode using the Voltera series, and developed nonlinear models for the transfer functions of second-harmonic, third-harmonic and two-tone third-order intermodulation distortions.

Morthier et al. [6] reported the numerical calculations of the second-order harmonic distortion in the amplitude modulation-response of Fabry-Perot and distributed feedback lasers, and studied the influence of several nonlinearities, such as longitudinal spatial hole burning, gain suppression and relaxation oscillations. They showed that the distortion at a certain frequency exhibits a minimum, as a result of the combination of spatial hole burning and relaxation oscillation contributions. Westbrook [7] successfully employed the harmonic balance method, for the first time, to a semiconductor laser amplifier, and derived the residual effect of facet reflectivity on the electrical feed forward

1. *School of Electrical Engineering, Sharif University of Technology, Tehran, P.O. Box 11155-9363, Iran.*
*. *Corresponding author. E-mail: khorasani@sharif.edu*

Received 13 August 2008; received in revised form 29 December 2008; accepted 18 April 2009

linearization. In another report [8], Morthier found that the dependence of absorption on the carrier density might play a prominent role in the second-order distortion in the AM-response. Furthermore, he noticed the effect to be pronounced at high output powers. Frommer et al. [9] demonstrated a method for the modulation of semiconductor lasers, based on modulation of the optical confinement factor.

Yu et al. [10] developed a rate-equation model by which they were able to analyze the steady state and dynamic behavior of index guided vertical-cavity surface-emitting lasers. They studied the influence of size effects on the amplitude modulation response and second-order harmonic distortion, and found that a laser with a small core radius would exhibit a better modulation response and less harmonic distortion than that of a large waveguide device. However, there was a tradeoff between the output power and modulation efficiency of the lasers. Cartledge and Srinivasan [11] developed a technique for readily extracting values of the rate equation parameters, using measurements of the threshold current, optical power, resonance frequency and the damping factor for a bias current well above the threshold current. Salgado et al. [12] employed a nonlinear analysis to the intermodulation distortion of semiconductor lasers, and could show that the intrinsic parameters of the laser diodes could be recovered from experimental measurements of the intermodulation distortion. Sharaiha [13,14] applied a harmonic balance approach based on a perturbation method to study the nonlinear response of semiconductor optical amplifiers to the third order.

A technique for the extraction of laser rate equation parameters to be used in the simulation of high-speed optical telecommunication systems is presented by André et al. [15]. They claimed that their simulation using the extracted parameters is valid even for large current modulation and soliton pulses. Chen et al. [16] studied third-order intermodulation nonlinearity, and showed the possible cancellation of various nonlinear effects by choosing an appropriate distributed-feedback structure and facet conditions. Morthier et al. [17] investigated the occurrence of a second resonance frequency in distributed Bragg reflector laser diodes and the resulting high modulation bandwidth. They also theoretically studied the possibilities of large-signal digital modulation and the influence of different laser parameters.

Yildirim et al. [18] discussed the effect of feedback on the harmonic distortion of a single-mode laser diode. Ghoniemy et al. [19] introduced a comprehensive model for semiconductor laser characteristics, such as relaxation-oscillation peak frequency, modulation bandwidth, and evaluated their model under different conditions.

To the best of our knowledge, no one has considered the problem of harmonic content in the optical frequency response of a laser diode, from an optimization point of view. We have recently revisited [20,21] and obtained expressions for the harmonic distortions introduced into the output of a directly current-modulated laser diode. Here, we extend this approach and present a full nonlinear analysis of the rate equations of a directly current-modulated laser diode subject to a sinusoidal input current. The distribution of input power among harmonics is fully described. We also study the THD with respect to the power of the first harmonic, and show that the maxima of output power coincide with the maxima of THD. This would suggest a trade-off between distortion and modulation efficiency, quite in agreement with the work of Yu et al. [10]. The absolute maximum is shown to appear as the first harmonic resonant frequency due to the Lorentzian characteristic of the output power. The poles of harmonic powers and their dependence on the bias current are completely analyzed. Because of the square root dependence of the resonant frequency to the current, the bias current can be adjusted to obtain the desired relaxation resonance frequency. Furthermore, we calculate and rigorously show that there is an optimal operation point to obtain the maximum primary harmonic power.

In the theoretical formulations, we simulate a typical in-plane (edge-emitting) semiconductor heterostructure laser with realistic parameters deduced from experimental measurements [1]. We ignore the effect of mode competition, with the understanding that the diode laser under consideration is supposed to be single mode. Furthermore, the effect of gain compression has been neglected for simplicity; that is known to be partly due to spatial hole burning. Whereas this phenomenon plays an important role in Vertical-Cavity Surface Emitting Lasers (VCSELs) [22], it is usually negligible for in-plane lasers. We also disregard the effect of thermal variations in cavity which can be justified if the typical time-scale of electrical excitations is shorter than 1 μs [23,24].

THEORY

Typical Experimental Setup

Figure 1 illustrates the typical standard setup [25,26] which is widely used for characterization of laser diodes. We suppose that the laser diode is excited by an AC current source with amplitude I_1 and frequency ω, biased at the constant current I_0 by means of a bias-tee. The modulated laser output is coupled into an optical fiber and then into a semiconductor PIN diode, or Avalanche Photo-Diode (APD), biased through a simple bias network. The detected signal is amplified and fed into a spectrum analyzer.

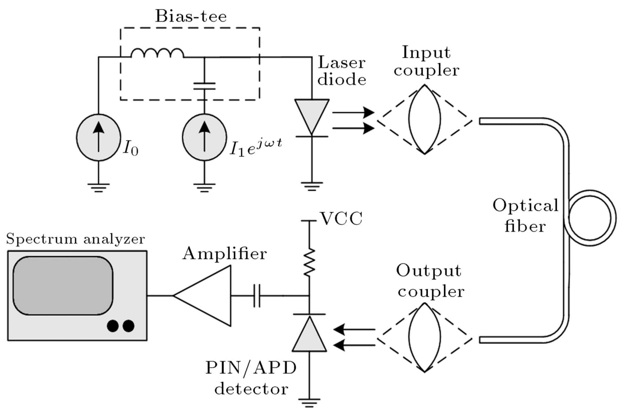

Figure 1. Typical experimental setup for measurement of harmonic distortion in modulation of laser diodes. A wideband PIN diode or Avalanche Photo Diode (APD) is used as the detector.

Theoretical Model

As discussed here, the employed physical model can explain the harmonic contents generated for a signal packet containing a frequency spectrum. The total electric current injected into the laser diode is given by:

$$I = I_0 + I_1 e^{j\omega t}. \tag{1}$$

We let the spatially-averaged photon and electron densities in the laser cavity be denoted, respectively, by N_P and N_E, whose harmonic contents are sought in this analysis. Expanding N_P and N_E as a Fourier series allows us to write:

$$N_E = \sum_{n=0}^{\infty} N_{E_n} e^{jn\omega t}, \tag{2}$$

$$N_P = \sum_{n=0}^{\infty} N_{P_n} e^{jn\omega t}, \tag{3}$$

where N_{P_n} and N_{E_n} are the corresponding expansion coefficients of the photon and electron densities, respectively.

Harmonic Density Contents

The well-known rate equations for an in-plane single mode laser diode are:

$$\frac{dN_E}{dt} = \eta \frac{I}{qV} - \frac{N_E}{\tau_e} - V_g a (N_E - N_{tr}) N_P,$$

$$\frac{dN_P}{dt} = \Gamma V_g a (N_E - N_{tr}) N_P - \frac{N_P}{\tau_p}, \tag{4}$$

where η_i is the efficiency coefficient; τ_e is the carrier lifetime; a is the differential gain; N_{tr} is the threshold electron density; Γ is the cavity confinement factor; V_g is the cavity volume; and τ_p is the photon lifetime.

We start our approach by substituting Equations 1 to 3 in Equations 4 which results in:

$$j\omega \sum_{n=1}^{\infty} N_{E_n} n e^{jn\omega t} = \eta_i \frac{I_0 + I_1 e^{j\omega t}}{qV} - \frac{1}{\tau_e} \sum_{n=0}^{\infty} N_{E_n} e^{jn\omega t}$$
$$- V_g a \left(\sum_{n=0}^{\infty} N_{E_n} e^{jn\omega t} - N_{tr} \right) \sum_{n=0}^{\infty} N_{P_n} e^{jn\omega t},$$

$$j\omega \sum_{n=1}^{\infty} N_{P_n} n e^{jn\omega t}$$
$$= \Gamma V_g a \left(\sum_{n=0}^{\infty} N_{E_n} e^{jn\omega t} - N_{tr} \right) \sum_{n=0}^{\infty} N_{P_n} e^{jn\omega t}$$
$$- \frac{1}{\tau_P} \sum_{n=0}^{\infty} N_{P_n} e^{jn\omega t}. \tag{5}$$

From DC Analysis ($n = 0$), however, we have:

$$N_{E_0} = \frac{\eta_i \frac{I_0}{qV} + V_g a N_{tr} N_{P_0}}{\frac{1}{\tau_e} + V_g a N_{P_0}},$$

$$\frac{1}{\Gamma \tau_P} = V_g a (N - N_{tr}). \tag{6}$$

The first harmonic of the photon density is generated directly by the first harmonic of the current applied to the laser diode, and we easily obtain:

$$N_{E_1} = \frac{\eta_i \frac{I_1}{qV}}{j\omega + \frac{1}{\tau_e} + V_g a N_{P_0} \left(1 + \frac{1}{j\omega \tau_p}\right)},$$

$$N_{P_1} = \frac{\Gamma V_g a N_{P_0}}{j\omega} N_{E_1}. \tag{7}$$

Higher harmonics are found from recursive equations which in the general case for an arbitrary integer, $k > 1$, may be written as:

$$jk\omega N_{E_k} = -\frac{N_{E_k}}{\tau_e} - V_g a \Bigg[(N_{E_0} - N_{tr}) N_{P_k}$$
$$+ N_{E_k} N_{P_0} + \sum_{n=1}^{k-1} N_{E_n} N_{P_{k-n}} \Bigg],$$

$$jk\omega N_{P_k} = \Gamma V_g a \left(N_{E_k} N_{P_0} + \sum_{n=1}^{k-1} N_{E_n} N_{P_{k-n}} \right). \tag{8}$$

Hence, the kth harmonic of the photon density may be calculated, once all the lower harmonics of photon and electron densities are known. We define the parameter, M_k, as the summation given at the right hand side of Equations 8 which relates the kth harmonic to the lower ones:

$$M_k \triangleq \sum_{n=1}^{k-1} N_{E_n} N_{P_{k-n}}. \tag{9}$$

Therefore, we can find the kth harmonics of the photon and electron densities as:

$$N_{E_k} = \frac{-V_g a\left(1+\frac{1}{jk\omega\tau_p}\right)}{jk\omega+\frac{1}{\tau_e}+V_g a N_{P_0}\left(1+\frac{1}{jk\omega\tau_p}\right)} M_k,$$

$$N_{P_k} = \frac{\Gamma V_g a}{jk\omega}(N_{P_0} N_{E_k} + M_k). \tag{10}$$

Harmonic Power Contents

In this section, we calculate the power content of each harmonic with relatively straightforward substitutions. To obtain the power contents, we first construct the stored optical energy in the cavity by multiplying the photon density, N_P, by the energy per photon, $h\nu$, and the cavity volume, V_p. Then, we multiply the product by the energy loss rate through the mirrors to get the optical power output; the mirror loss rate, α_m, is related to the mirror loss time, τ_m, as $\tau_m^{-1} = \alpha_m V_g$. Hence, the optical output power for the kth harmonic is given by:

$$P_k = P_{\text{out}_k} = \frac{h\nu V_p}{\tau_m} N_{p_k}. \tag{11}$$

By performing a summation on k, we obtain the Total Output Power:

$$P_{\text{out}}\big|_{\text{Total}} = \sum_k \frac{h\nu V_p}{\tau_m} N_{p_k}. \tag{12}$$

Total Harmonic Distortion (THD)

Amplitudes of photon and electron density harmonics, due to a single frequency excitation, may be successively calculated from Equations 10. Here, we define a parameter called the modulation index (denoted here by f) in contrast to the communication applications of this area, which satisfies the relation:

$$I_1 = f.I_0. \tag{13}$$

We, furthermore, define the THD as:

$$\text{THD} \triangleq \sqrt{\frac{\sum\limits_{n=2}^{\infty} |P_n(j\omega)|^2}{|P_1(j\omega)|^2}}. \tag{14}$$

This allows us to investigate the harmonic content versus the modulation index, in order to find the optimum THD. This is discussed in the next section.

Relaxation Resonant Frequency

The frequency, ω_R, at which the amplitude of the power harmonic content reaches its maximum is called the Relaxation Resonant Frequency. From Equations 7 the primary harmonic of the photon density is obtained as:

$$N_{P_1} = \frac{\Gamma V_g a N_{P_0}}{j\omega} \frac{\eta_i \frac{I_1}{qV}}{j\omega + \frac{1}{\tau_e} + V_g a N_{P_0}\left(1+\frac{1}{j\omega\tau_p}\right)}. \tag{15}$$

By simplification and applying Equation 11, we get:

$$P_1(j\omega) = \frac{h\nu V_p}{\tau_m}\left(\frac{\Gamma V_g a N_{P_0}\eta_i \frac{I_1}{qV}}{-\omega^2+\frac{j\omega}{\tau_e}+\frac{V_g a N_{P_0}}{\tau_p}(j\omega\tau_p+1)}\right). \tag{16}$$

The cavity confinement factor, Γ, is equal to the ratio, V/V_p; therefore, the above can be written as:

$$\frac{P_1(j\omega)}{I_1(j\omega)} = \frac{h\nu V_g a N_{P_0}\eta_i \frac{1}{\tau_m q}}{-\omega^2+\frac{j\omega}{\tau_e}+\frac{V_g a N_{P_0}}{\tau_p}(j\omega\tau_p+1)}. \tag{17}$$

By separating the real and imaginary parts of the denominator of Equation 17, we finally get:

$$\frac{P_1(j\omega)}{I_1(j\omega)} = \frac{h\nu V_g a N_{P_0}\eta_i \frac{1}{\tau_m q}}{\frac{V_g a N_{P_0}}{\tau_p} - \omega^2 + j\omega\left(\frac{1}{\tau_e}+V_g a N_{P_0}\right)}. \tag{18}$$

This expression clearly has two poles at:

$$\omega = \pm\left[\frac{1}{\tau_p}V_g a N_{P_0} - \frac{1}{4}\left(\frac{1}{\tau_e}+V_g a N_{P_0}\right)^2\right]^{\frac{1}{2}} + j\frac{1}{2}\left(\frac{1}{\tau_e}+V_g a N_{P_0}\right), \tag{19}$$

which are located in the first and second quadrants of the complex ω plane. We now notice that the real part of the denominator of Equation 18 becomes zero at the frequency:

$$\omega^2 = \omega_R^2 = \frac{V_g a N_{P_0}}{\tau_P}, \tag{20}$$

where ω_R is called the Relaxation Resonant Frequency. Since usually $\frac{1}{\tau_p} + V_g a N_{P_0} << \omega_R$ holds, we conclude that the magnitude of Equation 18 also reaches a maximum when $\omega \sim \omega_R$. Hence, the denominator becomes purely imaginary, and the primary power harmonic content reaches its resonance mode. We can apply this approach in finding the higher harmonic resonance frequencies as explained below.

Following the same approach, we find the second harmonic resonant frequency by substituting the second index in the rate equations (Equations 8). This results in:

$$2j\omega N_{E_2} = -\frac{N_{E_2}}{\tau_e} - \frac{N_{P_2}}{\Gamma\tau_P} - V_g a N_{E_2} N_{P_0} - V_g a N_{E_1} N_{P_1},$$

$$2j\omega N_{P_2} = \Gamma V_g a N_{E_2} N_{P_0} + \Gamma V_g a N_{E_1} N_{P_1} + \frac{N_{P_2}}{\tau_P} - \frac{N_{P_2}}{\tau_P}. \tag{21}$$

Rewriting the above equations in matrix form gives:

$$\begin{bmatrix} 2j\omega & -\Gamma V_g a N_{P_0} \\ \frac{1}{\Gamma\tau_P} & 2j\omega+\frac{1}{\tau_e}+V_g a N_{P_0} \end{bmatrix} \begin{bmatrix} N_{P_2} \\ N_{E_2} \end{bmatrix} = \begin{bmatrix} \Gamma V_g N_{E_1} N_{P_1} \\ -V_g a N_{E_1} N_{P_1} \end{bmatrix}. \tag{22}$$

If we want to compute the corresponding resonance frequencies, we have to find the frequency response of the second harmonic power; here, we must consider that the poles of $P_2(j\omega)$ are the same poles of N_{P_2}. For this purpose, we now define the matrix of coefficients at the left hand side of Equation 22 as:

$$A = \begin{bmatrix} 2j\omega & -\Gamma V_g a N_{P_0} \\ \frac{1}{\Gamma\tau_P} & 2j\omega + \frac{1}{\tau_e} + V_g a N_{P_0} \end{bmatrix}. \tag{23}$$

Considering Equation 22, it can be concluded that the poles of the second harmonic power include the poles of N_{E_1}/I_1 and N_{P_1}/I_1. In fact, the roots of the matrix equation, $|A| = 0$, characterize the rest of the poles:

$$\begin{aligned} |A| &= 2j\omega\left(2j\omega + \frac{1}{\tau_e} + V_g a N_{P_0}\right) + \frac{V_g a N_{P_0}}{\tau_P} \\ &= -4\omega^2 + \frac{V_g a N_{p_0}}{\tau_p} + j2\omega\left(\frac{1}{\tau_e} + V_g a N_{p_0}\right) \\ &= -4\omega^2 + \omega_{R_1}^2 + j2\omega\left(\frac{1}{\tau_e} + V_g a N_{p_0}\right) = 0. \end{aligned} \tag{24}$$

Consequently, we have:

$$P_2(j\omega) = \frac{A_1}{\left\{1-\left(\frac{\omega}{\omega_{R_1}}\right)^2 + j\left(\frac{\omega}{\omega_{R_1}}\right)\left[\omega_{R_1}\tau_P + \frac{1}{\tau_e\omega_{R_1}}\right]\right\}^2} \times \frac{A_2}{1-\left(\frac{2\omega}{\omega_{R_1}}\right)^2 + j\left(\frac{2\omega}{\omega_{R_1}}\right)\left[\omega_{R_1}\tau_P + \frac{1}{\tau_e\omega_{R_1}}\right]}, \tag{25}$$

where:

$$A_1 = \frac{h\nu V_g a N_{P_0}\eta_i \frac{1}{\tau_m q}}{\omega_{R_1}^2},$$

$$A_2 = \frac{-2V_g\eta_i\frac{1}{qV_p}}{\omega_{R_1}^2}\omega\left[\omega - \frac{j}{2}\left(\frac{1}{\tau_e} + \omega_{R_1}^2\tau_p(1+a)\right)\right] I_1^2. \tag{26}$$

Therefore, it can be concluded that the second harmonic power, $P_2(j\omega)$, has two resonance frequencies: ω_{R_1} and ω_{R_2}. We refer to ω_{R_2} as the second relaxation resonance frequency. Furthermore, Equation 25 yields:

$$\omega_{R_2} = \frac{1}{2}\omega_{R_1} = \frac{1}{2}\omega_R, \tag{27}$$

in which ω_R is given in Equation 20. As will be discussed in the next section, our simulations justify the above result.

If we continue this approach for higher harmonics, the rest of the poles similar to the poles of Equation 25 appear for the nth harmonic, in addition to the lower harmonic poles. This happens because the coefficient matrix of the nth harmonics:

$$A(nj\omega) = \begin{bmatrix} nj\omega & -\Gamma V_g a N_{p_0} \\ \frac{1}{\Gamma\tau_p} & nj\omega + \frac{1}{\tau_p} + V_g a N_{p_0} \end{bmatrix}, \tag{28}$$

needs to be inverted and multiplied by the right hand side of the corresponding set of equations. Hence, the poles given by the zeros of the determinant:

$$|A(nj\omega)| = \omega_{R_1}^2 - (n\omega)^2 + j(\omega_{R_1} n\omega)\left[\omega_{R_1}\tau_P + \frac{1}{\tau_e\omega_{R_1}}\right], \tag{29}$$

add up to the poles already generated by lower order harmonics. This causes the nth resonance frequency to be simply given by:

$$\omega_{R_n} = \frac{1}{n}\omega_{R_1}. \tag{30}$$

Due to the dominant fundamental pole at ω_{R_1}, with high recurrence in the denominator of the nth harmonic power, $P_n(j\omega)$, one has:

$$P_n(j\omega)\big|_{\omega=\omega_{R_n}} < P_n(j\omega)\big|_{\omega=\omega_{R_1}}, \tag{31}$$

which means that each harmonic still has its absolute maximum at the first resonant frequency of the laser diode.

Optimal Operation Point for Modulation

As discussed earlier, the optimum modulation frequency is the resonant frequency, which is determined from the bias current. Therefore, the optimal operation point for modulation where the power of the primary harmonic reaches its maximum must lie on the curve obtained from the following [1]:

$$\omega_{R_1}^2 = \frac{V_g a}{q V_P} \eta_i (I_o - I_{th}). \tag{32}$$

Hence, if we apply Relation 32 into Equation 18, and simplify the result, the peak curve of the first harmonic power will be determined merely by the modulation frequency (which is already set at the resonant frequency):

$$\frac{P_1(j\omega)}{I_1(j\omega)} = -j \frac{h\nu\eta_i}{\tau_m q} \cdot \frac{\omega_{R_1}}{\omega_{R_1}^2 + \frac{1}{\tau_e \tau_p}}. \tag{33}$$

The above equation is not monotonic with respect to frequency, and has a maximum value that is determined by derivation with respect to the modulation frequency. This maximum value occurs at:

$$\omega_{R_{\text{Optimum}}} = \frac{1}{\sqrt{\tau_e \tau_P}}, \tag{34}$$

which yields the optimum bias current by using Equation 32 as:

$$I_{0_{\text{Optimum}}} = I_{th} + \frac{q V_P}{V_g a \eta_i \tau_e \tau_P}. \tag{35}$$

By increasing the bias current over the threshold, as shown in the above equation, and using the modulation frequency given by Equation 34, the optimal operation point is found.

As a result, the maximum value of the first harmonic power is given by:

$$\left(\frac{P_1(j\omega)}{I_1(j\omega)} \right)_{\max} = -j \frac{h\nu\eta_i}{2\tau_m q \sqrt{\tau_e \tau_p}}. \tag{36}$$

RESULTS AND DISCUSSION

THD Analysis

Locations of poles in the complex space for the first four harmonic powers of a typical laser diode are shown in Figure 2. By increasing the bias current, the distance of poles from the origin increases. The numerical values of all physical parameters of the laser diode are listed in Table 1 (taken from [1, pp. 198-199]).

Variations of THD versus the frequency and modulation current are shown in Figures 3a and 3b, respectively. As we increase the modulation current, THD increases rapidly and, even for higher values of modulation current, it grows faster.

Resonance frequencies are evident in Figure 3b around which the THD undergoes a local or global maximum; this confirms our theoretical predictions. Counting from the higher frequencies, the first peak

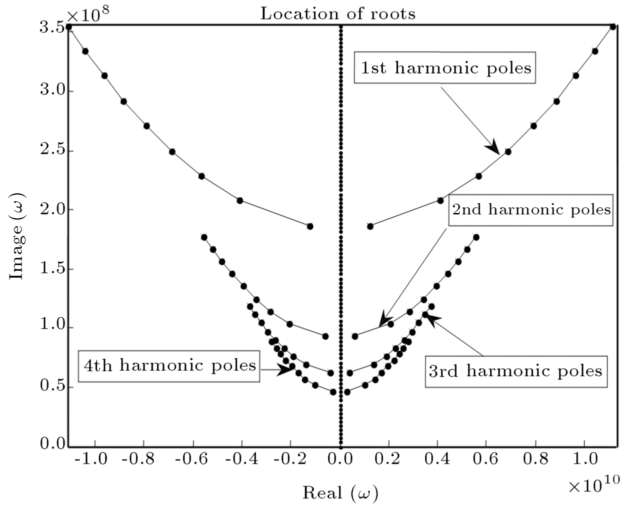

Figure 2. Location of poles for the first four harmonics power contents of a laser diode.

Table 1. Parameters used for the in-plane laser [1, pp. 198-199].

Parameter	Value
η_i	0.8
a	5.34×10^{-16} cm^{-2}
N_{tr}	1.8×10^{18} cm^{-3}
V_g	3×10^{10} cm/s
Γ	0.032
τ_e	2.71 ns
τ_p	2.77 ps
α_m	45.6 cm^{-1}

exactly coincides with the first resonant frequency calculated from the approach (around 2.9 GHz), and the second peak coincides with second resonant frequency (around 1.46 $\approx$ 2.9/2 GHz). The rest of the resonant frequencies also present distortions to the THD, however, with a much smaller effect. For example, the effect of the third resonant frequency (approximately 0.97 $\approx$ 2.9/3 GHz) can be seen in Figure 3b as a very small bend around 1 GHz.

Obviously, harmonic contents greatly vary, with respect to the modulation current and its frequency. Generally speaking, higher harmonic contents tend to increase with modulation current and frequency, but the variations of second and third harmonics are not monotonic. In some cases, as shown in Figure 4, the third harmonic power is higher than that of the second harmonic.

The variations of the power harmonic content versus frequency and bias current are also shown in Figure 5. As explained earlier, the variation of power harmonic versus frequency is not monotonic; for instance at $\omega = 1.6$ GHz, the second power harmonic is

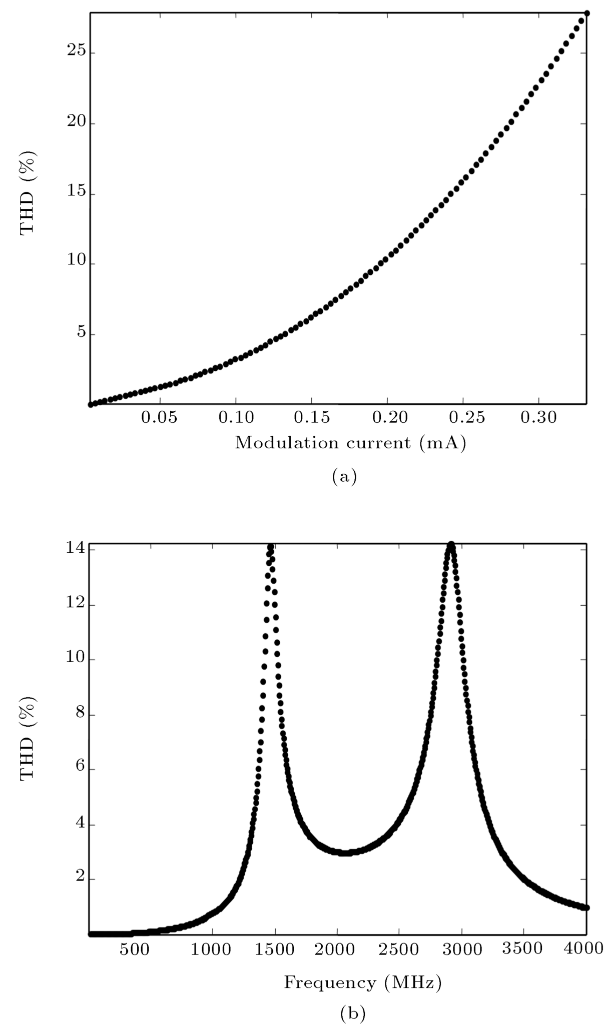

Figure 3. Total Harmonic Distortion (THD); bias current is 3.31 mA. (a) THD vs. modulation current at the modulation frequency of 1 GHz; (b) THD vs. frequency at the modulation current of 33.1 μA.

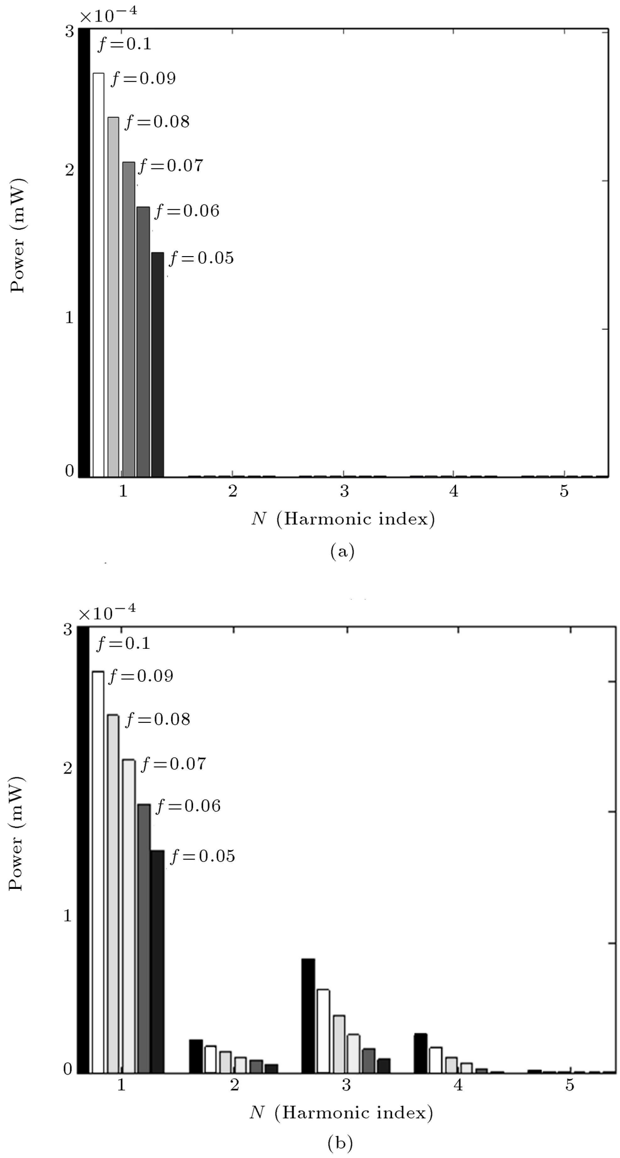

Figure 4. Power harmonic content versus harmonic index number for different values of current modulation index. (a) Modulation frequency is 100 MHz; (b) Modulation frequency is 1 GHz.

dominant compared to the other frequencies, but these power variations appear to be monotonous in the case of a bias current.

First and Second Harmonic Powers

We have seen that the optical output power of each harmonic is a function of frequency and the input current, such as:

$$P_{\mathrm{out}_k} = f(\omega, I). \tag{37}$$

Besides, the relationship of optical output power with frequency and current is in the form of a Lorentzian function. The first resonance frequency itself is also related to the current by Equation 32, which means that all resonance frequencies are proportional to the square root of the bias current given by:

$$\omega_{R_n} \propto \sqrt{I_o - I_{th}}. \tag{38}$$

Now, we define ξ as:

$$\xi = \frac{V_g a}{qV_P}\eta_i. \tag{39}$$

This allows us to summarize the bilateral dependence of frequency and current in the optical output power formula as follows:

$$\frac{P_1(j\omega)}{I_1(j\omega)} = \frac{\eta_d \frac{hv}{q}}{1 - \frac{\omega^2}{\xi^2(I_o - I_{th})} + j\omega\tau_P + j\frac{1}{\tau_e\xi(I_o - I_{th})}}. \tag{40}$$

The dependence of P_1 related to ω and I_0 is obvious in Equation 40. We obtain a surface by plotting the optical output power per various bias currents and

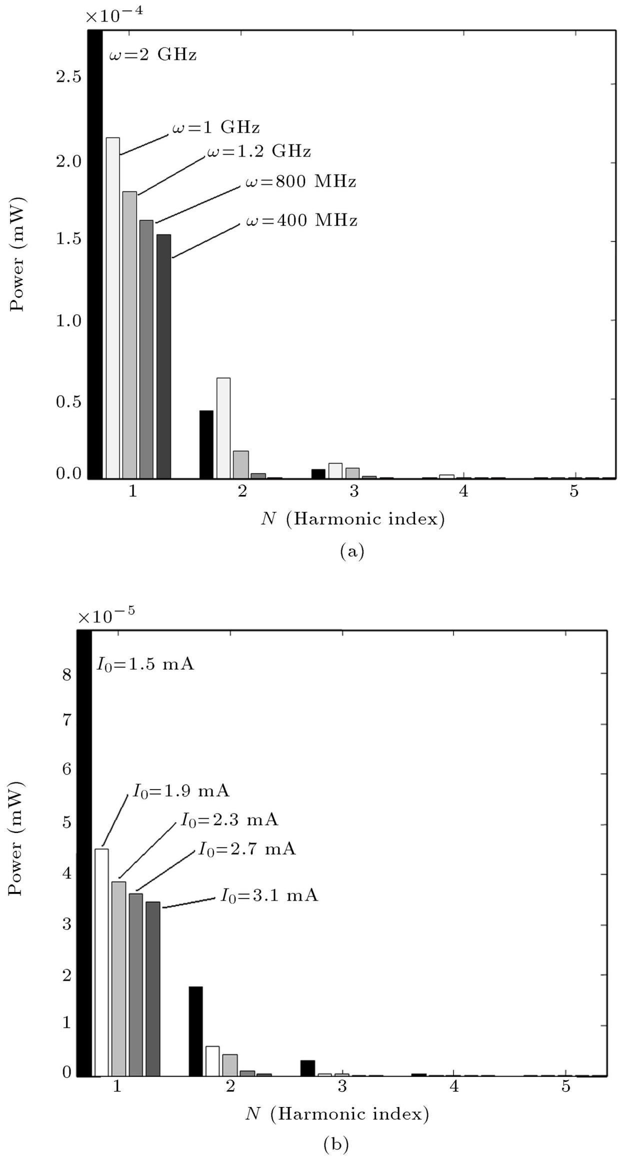

Figure 5. Power harmonic content versus harmonic index number; (a) Effect of frequency; (b) Effect of bias current.

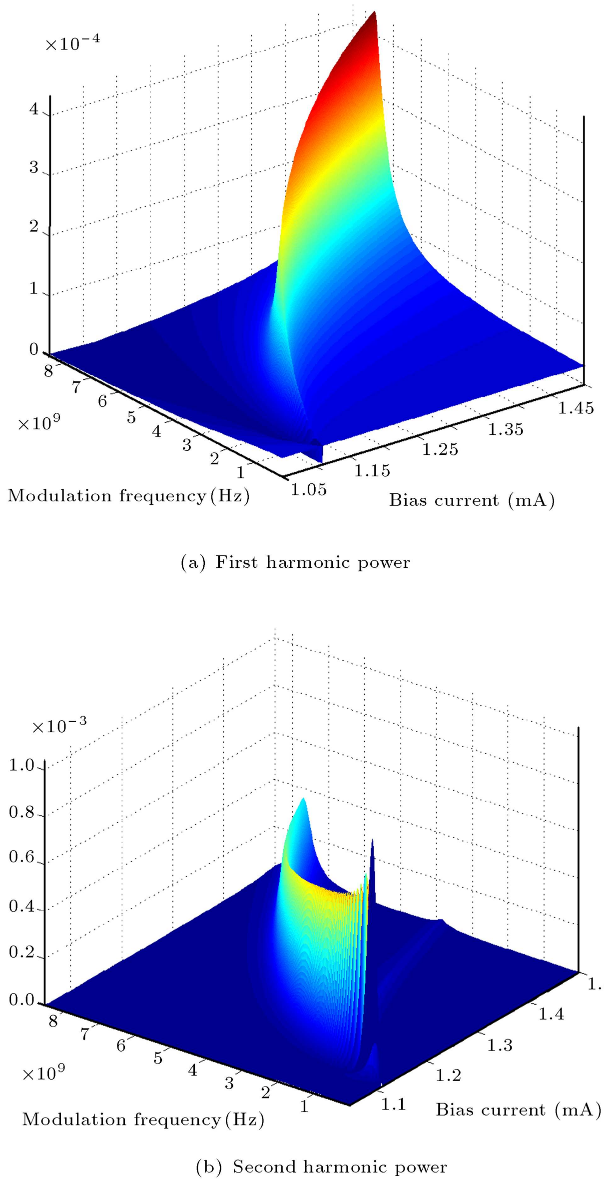

Figure 6. Plots of (a) First harmonic power $P_1(j\omega)$; and (b) Second harmonic power $P_2(j\omega)$, vs. frequency and bias current ($I_{\text{th}} = 1.11$ mA).

excitation frequencies in Figure 6. The maximum amplitudes lie on a peak curve given by the resonant frequency equation:

$$\omega = \omega_{R_1} = \xi\sqrt{I_o - I_{th}}. \tag{41}$$

This estimation is also in perfect agreement with numerical calculations. The dependence of ω_{R_1} in terms of bias current is also shown in Figure 6. As illustrated in Figure 6b, the primary and second resonance frequency peak curves exactly match with Equation 27. As discussed earlier, the second harmonic power on this curve is smaller and suppresses faster. The contour plots of first and second harmonic powers can be seen in Figure 7. As predicted before, in small currents near the threshold, the nonlinearity effect is larger and affects the second harmonic power to a large extent.

We have also extended the intervals of our input variables to higher ranges for investigating the trends of the first and second harmonic powers; this is shown in Figure 8. As demonstrated in the previous section, the trend of the first harmonic power on the peak curve (Equation 41) is not monotonic, and undergoes a maximum (which is already calculated); after passing this sole maximum, it diminishes slowly.

The second harmonic power decays quickly by increasing the bias current and modulation frequency. The contour plots of Figure 9 are again in complete agreement with previous formulae.

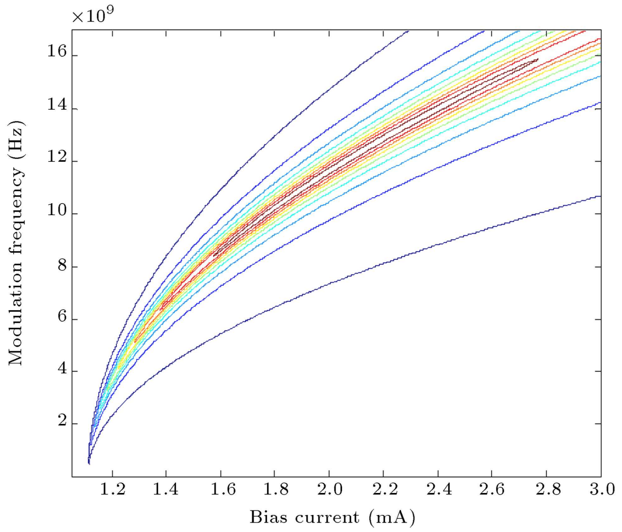

(a) First harmonic power $P_1\,(j\omega)$

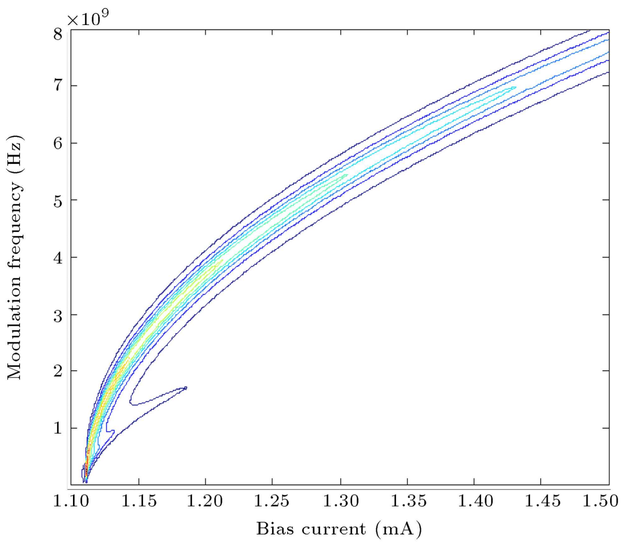

(b) Second harmonic power $P_2\,(j\omega)$

Figure 7. Contour plots of the (a) First harmonic power $P_1(j\omega)$; and (b) Second harmonic power $P_2(j\omega)$ vs. frequency and bias current ($I_{\text{th}} = 1.11$ mA).

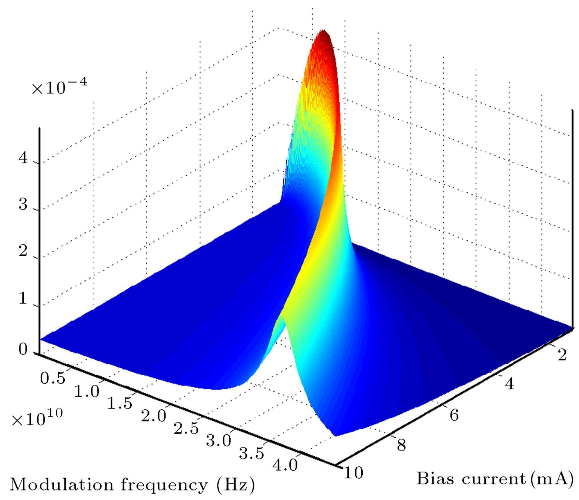

(a) First harmonic power

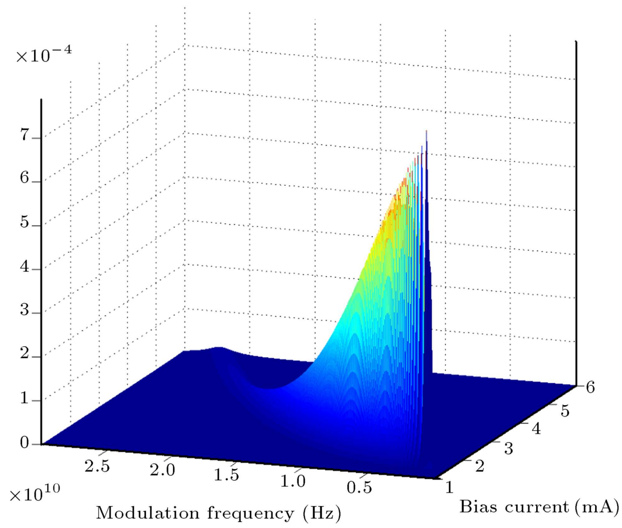

(b) Second harmonic power

Figure 8. Plots of (a) First harmonic power $P_1(j\omega)$; and (b) Second harmonic power $P_2(j\omega)$ vs. frequency and bias current ($I_{\text{th}} = 1.11$ mA).

Power Distribution Between Harmonics

The diagrams of harmonic powers are plotted in Figure 10 on the logarithmic scale. The first four resonance frequencies are shown for comparison. At bias currents near to the threshold, we observe that because of high nonlinearity the power of the upper harmonics (second, third, and fourth) exceed the power of the first harmonic in frequencies near the resonance frequencies. This point is illustrated in Figure 10a. If we increase the bias current, the power content of upper harmonics suppresses as shown in Figure 10b. If the bias current is increased further, the power of the higher harmonics diminishes very fast and thus can be neglected.

In order to distinguish the share of each harmonic in the total power applied to the laser diode, the percentages of power distribution in the first four harmonics are shown in Figure 11. Here, to calculate the total power, we have considered a sufficient number of harmonics to reach convergence.

Similar to Figure 10, at the bias currents near the threshold, the higher harmonics absorb more power than the first one. Therefore, we expect to observe distortions near the threshold. If we increase the bias current further, the higher harmonics suppress to negligible percentages. The relating diagrams are shown in Figures 11a and 11b, respectively.

The amplitudes of the first and the second harmonics on the peak curve (Equation 41) are plotted

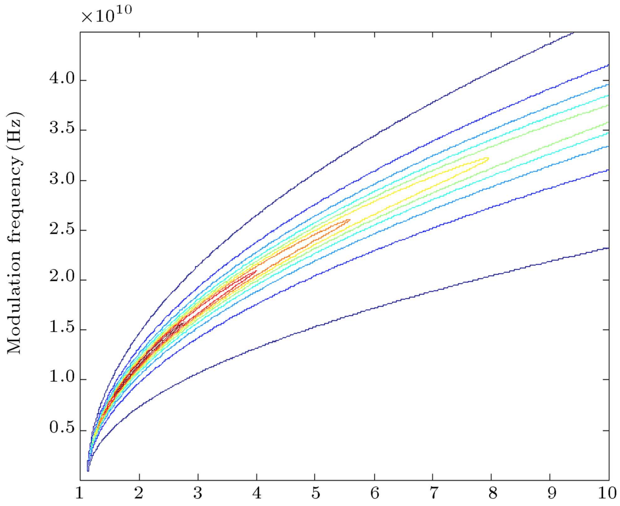

(a) First harmonic power $P_1(j\omega)$

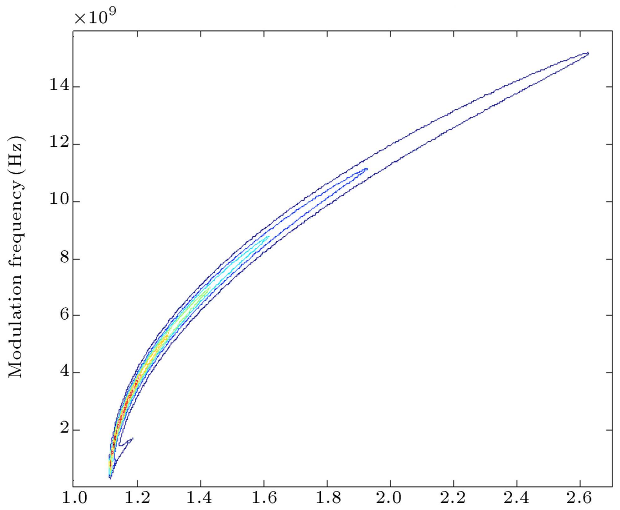

(b) Second harmonic power $P_2(j\omega)$

Figure 9. Contour plots of the (a) First harmonic power $P_1(j\omega)$; and (b) Second harmonic power $P_2(j\omega)$ vs. frequency and bias current ($I_{\text{th}} = 1.11$ mA).

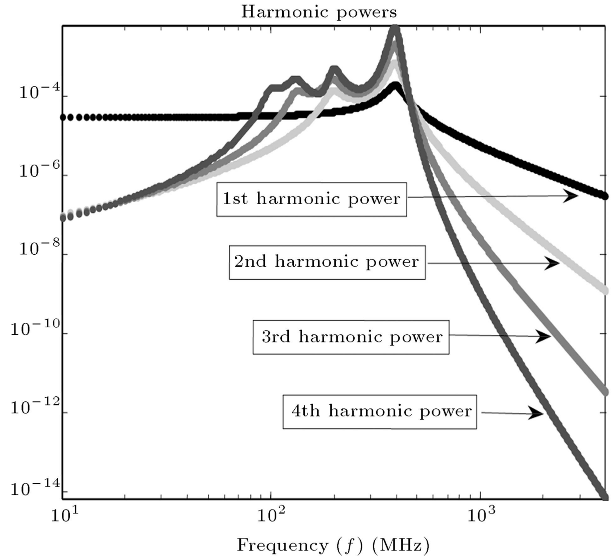

(a)

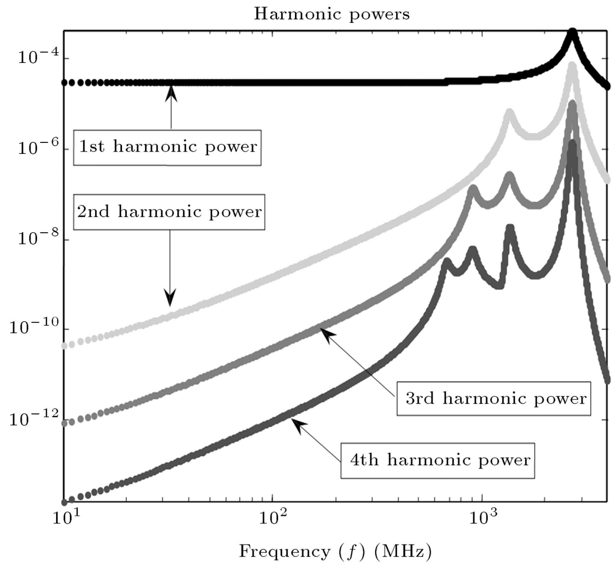

(b)

Figure 10. Harmonic power versus frequency. (a) Bias current: 1.15 mA; (b) Bias current: 3mA ($I_{\text{th}} = 1.11$ mA).

in Figure 12a. The optimal operation point for the first harmonic power calculated by Equation 39 exactly coincides with the point observed in this figure; although we anticipate distortions near the threshold, the second harmonic power is much higher than its expected value. This issue is observed more seriously also for higher harmonics. This is shown on a semi-logarithmic scale in Figure 12b. It seems that this situation cannot be satisfactorily explained by rate equations and, in practice, we expect the amplitude of the harmonic powers to be confined regardless of the distortions near the threshold current. Finally, the variations of THD with respect to the bias current on the peak curve (Equation 41), are plotted in Figure 13. As expected, the trend is descending too; in other words, by increasing the input power and tuning the modulation frequency at the resonance frequency, the system characteristics improve.

CONCLUSION

We have extracted an exact expression for the power of each harmonic and shown that the resonance frequency for the nth harmonic is proportional to the Relaxation Resonance Frequency of the first harmonic. The

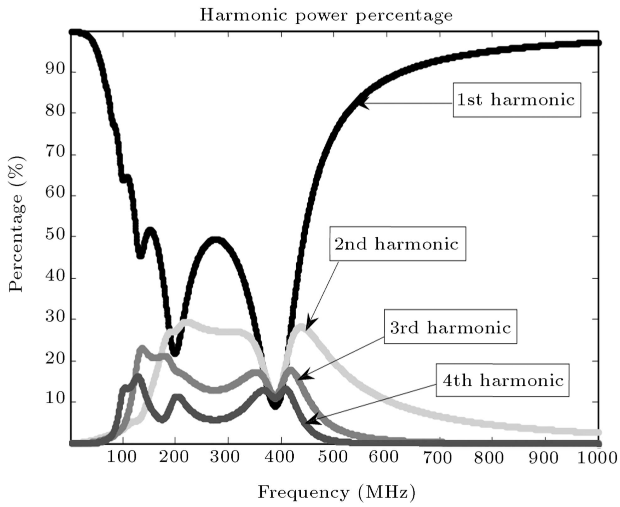

(a)

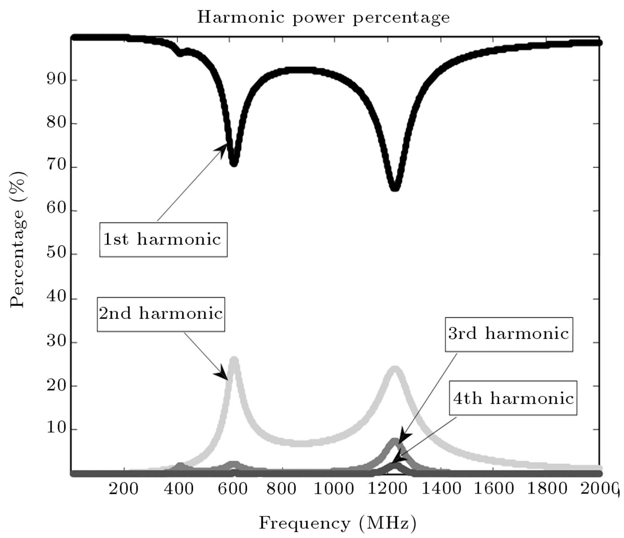

(b)

Figure 11. Harmonic power percentage over all harmonics versus frequency. (a) Bias current: 1.15 mA; (b) Bias current: 1.5 mA ($I_{\rm th} = 1.11$ mA).

THD, with respect to the power of the first harmonic, has been suitably defined and computed. We have shown that, due to its Lorentzian characteristic, the maximum of the optical output power occurs at the first harmonic's resonance frequency. Moreover, the square root dependence of the resonant frequency to the bias current allows one to tune the input current in order to obtain the desired Relaxation Resonance Frequency. The optimal operation point for gaining the highest primary harmonic power has been calculated. We conclude that, in general, increasing the bias current and modulation frequency suppresses the THD. The results of this study can be helpful in the design and optimization of nonlinear distortions which are naturally associated with the transmission of a signal by a semiconductor laser diode.

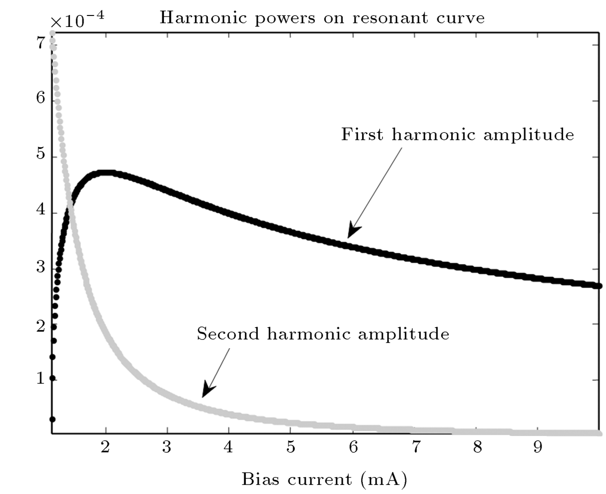

(a)

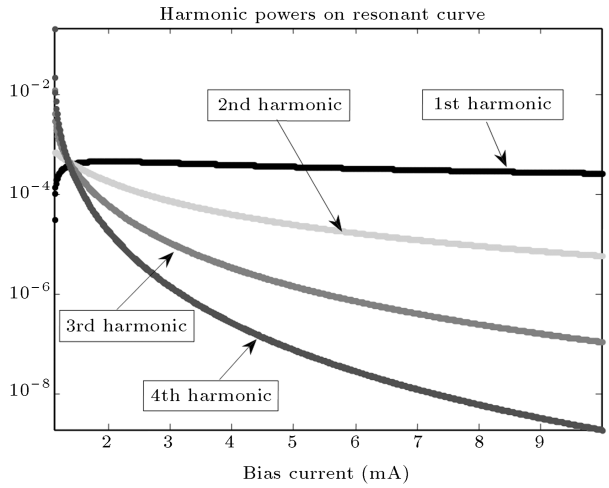

(b)

Figure 12. Harmonic powers on peak curve (first resonant frequency) versus bias current. (a) First and second harmonics; (b) First four harmonics in semi-logarithmic scale ($I_{\rm th} = 1.11$ mA).

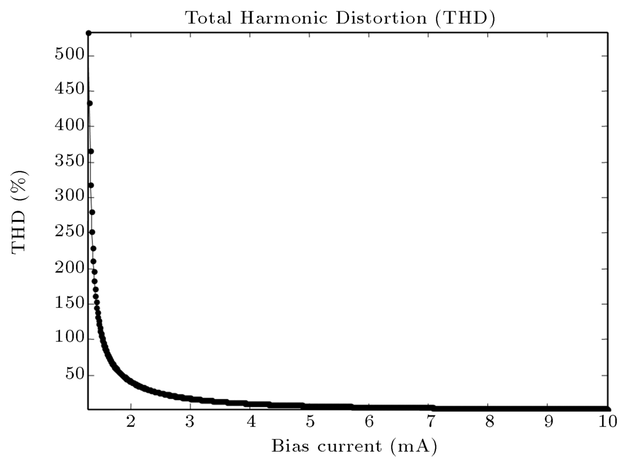

Figure 13. Total Harmonic Distortion (THD) on peak curve (first resonant frequency) versus the bias current ($I_{\rm th} = 1.11$ mA).

REFERENCES

1. Coldren, L.A. and Corzine, S.W., *Diode Lasers and Photonic Integrated Circuits*, John Wiley & Sons (1995).
2. Lance, C.H., Eom, J., Su, C.B., Schlafer, J. and Lauer, R.B. "Measurement of intrinsic frequency response of semiconductor lasers using optical modulation", *IEEE Elec. Lett.*, **24**(8), pp. 1131-1132 (1988).
3. Way, W.I. "Large signal nonlinear distortion prediction for a single-mode laser diode under microwave intensity modulation", *J. Lightwave Technol.*, **5**(3), pp. 305-315 (1987).
4. Lin, M.S., Wang, S.-Y.J. and Dutta, N.K. "Measurements and modeling of the harmonic distortion in InGaAsP distributed feedback lasers", *IEEE J. Quantum Electron.*, **26**(6), pp. 998-1004 (1990).
5. Biswas, T.K. and McGee, W.F. "Volterra series analysis of semiconductor laser diode", *IEEE Photonics Technol. Lett.*, **3**(8), pp. 706-708 (1991).
6. Morthier, G., Libbrecht, F., David, K., Vankwikelberge, P. and Baets, R.G. "Theoretical investigation of the second-order harmonic distortion in the AM response of 1.55 μm $F-P$ and DFB lasers", *IEEE J. Quantum Electron.*, **27**(8), pp. 1990-2002 (1991).
7. Westbrook, L.D. "Simulation of semiconductor laser amplifiers using harmonic balance", *IEEE Electronic Lett.*, **28**(25), pp. 2348-2350 (1992).
8. Morthier, G. "Influence of the carrier density dependence of the absorption on the harmonic distortion in semiconductor lasers", *J. Lightwave Technol.*, **11**(1), pp. 16-19 (1993).
9. Frommer, A., Luryi, S., Nichols, D.T., Lopata, J. and Hobson, W.S. "Direct modulation and optical confinement factor modulation of semiconductor lasers", *Appl. Phys. Lett.*, **67**(12), pp. 1645-1647 (1995).
10. Yu, S.F., Wong, W.N., Shum, P. and Li, E.H. "Theoretical analysis of modulation response and second-order harmonic distortion in vertical-cavity surface-emitting lasers", *IEEE J. Quantum Electron.*, **32**(12), pp. 2139-2147 (1996).
11. Cartledge, J.C. and Srinivasan, R.C. "Extraction of DFB laser rate equation parameters for system simulation purposes", *J. Lightwave Technol.*, **15**(5), pp. 852-860 (1997).
12. Salgado, H.M., Ferreira, J.M. and O'Reilly, J.J. "Extraction of semiconductor intrinsic laser parameters by intermodulation distortion analysis", *IEEE Photonics Technol. Lett.*, **9**(10), pp. 1331-1333 (1997).
13. Sharaiha, A. "Harmonic and intermodulation distortion analysis by perturbation and harmonic balance methods for in-line photodetection in a semiconductor optical amplifier", *IEEE Photonics Technol. Lett.*, **10**(3), pp. 421-423 (1998).
14. Sharaiha, A. "Distortion analysis of the photodetection and gain spectral responses of a semiconductor optical amplifier", *IEEE Photonics Technol. Lett.*, **10**(9), pp. 1301-1303 (1998).
15. André, P.S., Nolasco Pinto, A., Pinto, J.L. and da Rocha, F. "Extraction of laser rate equations parameters", *Proc. SPIE* **3572**, pp. 141-146 (1999).
16. Chen, J., Ram, R.J. and Helkey, R. "Linearity and third-order intermodulation distortion in DFB semiconductor lasers", *IEEE J. Quantum Electron.*, **35**(8), pp. 1231-1237 (1999).
17. Morthier, G., Schatz, R. and Kjebon, O. "Extended modulation bandwidth of DBR and external cavity lasers by utilizing a cavity resonance for equalization", *IEEE J. Quantum Electron.*, **36**(12), pp. 1468-1475 (2000).
18. Yildirima, R. and Schetzen, M. "Applications of the single-mode laser-diode system theory", *Elsevier Optics Comm.*, **219**, pp. 351-355 (2002).
19. Ghoniemy, S., McEachern, L. and Mahmoud, S. "Extended robust semiconductor laser modeling for analog optical link simulations", *IEEE J. Sel. Topics Quantum Electron.*, **9**(3), pp. 872-878 (2003).
20. Zandi, H., Bavafa, M., Chamanzar, M. and Khorasani, S. "Analysis of power harmonic content and relaxation resonant frequency of a diode laser", *Proc. SPIE 6468(64680J)* (2007).
21. Bavafa, M., Zandi, H., Chamanzar, M. and Khorasani, S. "Optimum operation point for the primary harmonic content of a modulated laser diode", *Proc. 6th WSEAS Intl. Conf. on Microelectronics, Nanoelectronics, Optoelectronics (MINO'07)*, pp. 86-91 (2007).
22. Khorasani, S. and Cabon, B. "Theory of optimal mixing in directly modulated laser diodes", *Scientia Iranica, Transactions D*, **16**(2), pp. 157-162 (2009).
23. Gustavsson, J.S., Vukusic, J.A., Bengtsson, J. and Larsson, A. "A comprehensive model for the modal dynamics of vertical-cavity surface-emitting lasers", *IEEE J. Quantum Electron.*, **38**(2), pp. 203-212 (2002).
24. Gustavsson, J.S., Haglund, A., Bengtsson, J. and Larsson, A. "High-speed digital modulation characteristics of oxide-confined vertical-cavity surface-emitting lasers-numerical simulations consistent with experimental results", *IEEE J. Quantum Electron.*, **38**(8), pp. 1089-1096 (2002).
25. Le Guennec, Y., Maury, G., Yao, J. and Cabon, B. "New optical microwave up-conversion solution in radio-over-fiber networks for 60-GHz wireless applications", *J. Lightwave Technol.*, **24**(3), pp. 1277-1282 (2006).
26. Schimpf, A., Bucci, D. and Cabon, B. "Low cost optical up-conversion of IR-UWB signals beyond the relaxation frequency of a vertical cavity surface emitting laser (VCSEL)", *Proc. 2008 IEEE Int. Conf. Ultra-Wideband (ICUWB2008)*, **2**, pp. 25-28 (2008).